2. SHAFT SENSORLESS FORCED DYNAMICS CONTROL OF INDUCTION MOTOR DRIVES

2.1. Sensorless Induction Motor Drive Control System with Prescribed Closed-Loop Rotor Magnetic Flux and Speed Dynamics

Abstract: This section briefly describes the theory and presents experimental results of the new method for control of electric drives with induction motors presented in section 2.1. Control of the rotor magnetic flux norm and angular velocity is achieved without measurements from sensors mounted on the output shaft. The dynamic responses of both the controlled variables are of the first order with time constants chosen by the drive user to suit the particular application. The experimental results presented show good agreement with theoretical conclusions and simulation results obtained previously.

2.1.1 Introduction

In contrast with conventional approaches to electric drives with induction motors, the combined induction motor and load are viewed as a multivariable nonlinear plant, the *control* variables, *measurement* variables and *controlled* variables being, respectively, the *individual phase voltages*, the *stator currents*, and the *rotor magnetic flux and angular speed.*

The *linearising function* [1], the *block control principle* [2] and the *motion separation principle* [3], are combined to form a new non-linear multivariable drive control algorithm which achieves ideal de-coupling of the flux and speed control channels, assuming perfect estimates of the motor parameters.

A very important feature of the new control system is that it contains a closed-loop oscillatory mode, which automatically generates stator currents of variable magnitude and frequency such that the prescribed dynamic responses of the rotor speed and flux magnitude to their corresponding demanded values is achieved.

The other important feature, is that the system presented achieves *speed control of moderate accuracy without the need for a velocity sensor on the output shaft of the motor*. Observers produce estimates of the rotor magnetic flux components, rotor speed and load torque which are the variables required as inputs to the control law. This represents a significant innovation in the field of electric drives and for the first time, *the rotor speed and rotor magnetic flux magnitude* are *independently controlled* with *closed-loop time constants chosen by the control system designer.*

The system described in this chapter is a form of *feedback linearisation* but it should be noted that, in general, it is not restricted to linear closed-loop dynamics. It would be possible to form a control algorithm to make the closed-loop system obey any first order differential equation relating the rotor speed to its demand. For example, as required in some applications, the drive could be made to increase or decrease speed at prescribed constant accelerations and decelerations to reach new constant reference speeds. For this reason, the general title, *forced dynamic control,* is used to describe the general method. The reason for a linear choice of dynamics, however, is that a control system intended to incorporate the drive could be designed with the aid of linear control theory.

2.1.2 Control System Development

2a) Model of Induction Motor

One of the motivations for the new approach was to eliminate the on-line computation of time varying transformation matrices, as required in conventional vector control methods, and for this reason, the basis for the control system development is the following induction motor model, formulated in the stator-fixed α, β co-ordinate system:

$$\frac{d\omega_r}{dt}=\frac{1}{J_r}\left(\Gamma_{el}-\Gamma_L\right)=\frac{1}{J_r}\left\{\frac{3\,L_m}{2\,L_r}p\left[\psi_{r\alpha}\,i_{s\beta}-\psi_{r\beta}\,i_{s\alpha}\right]-\Gamma_L\right\} \qquad (2.1.1a)$$

$$\dot{\omega}_r = \frac{1}{J_r}\left(\Gamma_{el} - \Gamma_L\right) = \frac{1}{J_r}\left(c_5 \boldsymbol{\Psi}^T \mathbf{T}^T \mathbf{I} - \Gamma_L\right), \quad \dot{\Gamma}_L = 0 \tag{2.1.1b}$$

$$\frac{d\psi_{r\alpha}}{dt} = -\frac{1}{T_r}\psi_{r\alpha} - p\omega_r \psi_{r\beta} - \frac{L_m}{T_r} i_{s\alpha}$$

$$\frac{d\psi_{r\beta}}{dt} = -\frac{1}{T_r}\psi_{r\beta} + p\omega_r \psi_{r\alpha} + \frac{L_m}{T_r} i_{s\beta} \tag{2.1.2a}$$

$$\dot{\boldsymbol{\Psi}} = -\mathbf{P}(\omega_r)\boldsymbol{\Psi} + c_4 \mathbf{I} \tag{2.1.2b}$$

$$\frac{di_{s\alpha}}{dt} = \frac{L_r}{L_s L_r - L_m^2}\left\{ u_{s\alpha} - \left(R_s + \frac{L_m^2}{L_r T_r}\right) i_{s\alpha} - \frac{L_m}{L_r}\left[\frac{-1}{T_r}\psi_{r\alpha} - p\omega_r \psi_{r\beta}\right]\right\}$$

$$\frac{di_{s\beta}}{dt} = \frac{L_r}{L_s L_r - L_m^2}\left\{ u_{s\beta} - \left(R_s + \frac{L_m^2}{L_r T_r}\right) i_{s\beta} - \frac{L_m}{L_r}\left[\frac{-1}{T_r}\psi_{r\beta} + p\omega_r \psi_{r\alpha}\right]\right\} \tag{2.1.3a}$$

$$\dot{\mathbf{I}} = c_1\left[c_2 \mathbf{P}(\omega_r)\boldsymbol{\Psi} - a_1 \mathbf{I} + \mathbf{U}\right], \tag{2.1.3b}$$

where $\boldsymbol{\Psi}^T = [\Psi_\alpha \ \Psi_\beta]$ is the rotor magnetic flux, $\mathbf{I}^T = [\imath_\alpha \ \imath_\beta]$ is the stator current, $\mathbf{U}^T = [u_\alpha \ u_\beta]$ is the stator voltage, $\boldsymbol{\Gamma}_{el}$ is the torque developed by the motor, ω_r is the mechanical rotor speed, and individual constants are given by: $c_1 = L_r/(L_s L_r - L^2_m)$, $c_2 = L_m/L_r$, $c_3 = R_r/L_r = 1/T_r$, $c_4 = L_m/T_r$, $c_5 = 1{,}5.p.L_m/L_r$ and $a_1 = R_s + (L^2_m/L^2_r)R_r$, where L_s , L_r and L_m are, respectively, the stator and rotor inductance and their mutual inductance. R_s and R_r are, respectively, the stator and rotor resistance and p is the number of stator pole pairs. Also,

$$\mathbf{P}(\omega_r) = \begin{bmatrix} c_3 & p\omega_r \\ -p\omega_r & c_3 \end{bmatrix}, \tag{2.1.4a}$$

$$\mathbf{T} = \begin{bmatrix} 0 & -1 \\ 1 & 0 \end{bmatrix}. \tag{2.1.4b}$$

Since all currents referred to are stator currents and all the magnetic fluxes are rotor fluxes, the corresponding subscripts, r and s, in the following equations will be omitted

2b) The Control Law Derivation

2b1) Approach

The control law synthesis is carried out in two stages. First, the current vector, **I**, is regarded as a *fictitious control vector*. The *master control law* is then formed for controlling the rotor speed and maintaining a substantially constant rotor magnetic flux magnitude independently. The fictitious control variables are made non-linear functions of the state variables and the reference inputs such that the differential equations relating the controlled variables to the corresponding reference inputs are *linear* with the *desired dynamic characteristics*. These functions are referred to as *linearising functions*. Second, a robust (either high gain or sliding mode) control law, denoted the *slave control law*, is formed, with the stator voltage vector, **U**, as the control vector to ensure that the true current vector, **I**, closely follows the demanded current vector, $\mathbf{I_d}$. This is implemented using a current fed inverter.

2b2) Rotor speed linearising function

The desired closed-loop linear differential equation is:

$$\dot{\omega}_r = \frac{1}{T_\omega}\left(\omega_d - \omega_r\right), \tag{2.1.5}$$

where $\omega_d(t)$ is the demanded angular velocity and T_ω is the closed-loop time constant. The linearising function is chosen to force the non-linear differential equation (2.1.1) to have the same response as the linear differential equation (2.1.5). This is achieved by equating the right hand sides of these equations, yielding the following linearising function:

$$\mathbf{\Psi}^T\mathbf{T}^T\mathbf{I} = \frac{1}{c_5}\left[\frac{J}{T_\omega}\left(\omega_d - \omega_r\right) + \Gamma_L\right]. \tag{2.1.6}$$

2b3) Rotor magnetic flux linearising function

A convenient norm for the rotor flux vector is the *square* of its magnitude, $\|\Psi\| = \Psi^T\Psi$. First equation (2.1.2) is expressed in terms of $\|\Psi\|$ using equation (2.1.4) for $\mathbf{P}(\omega_r)$. Thus:

$$\dot{\|\Psi\|} = \boldsymbol{\Psi}^T\left[-\mathbf{P}(\omega_r)\boldsymbol{\Psi} + c_4\mathbf{I}\right] + \left[-\boldsymbol{\Psi}^T\mathbf{P}^T(\omega_r) + c_4\mathbf{I}^T\right]\boldsymbol{\Psi}. \tag{2.1.7}$$

Hence

$$\dot{\|\Psi\|} = -2\left(c_3\|\Psi\| - c_4\boldsymbol{\Psi}^T\mathbf{I}\right). \tag{2.1.8}$$

The linearising function is formulated to yield a first order linear dynamic response of $\|\Psi\|(t)$ to a demand, $\|\Psi\|_d$, with a time constant, T_Ψ. Thus:

$$\dot{\|\Psi\|} = \frac{1}{T_\Psi}\left(\|\Psi\|_d - \|\Psi\|\right). \tag{2.1.9}$$

Equating the right hand sides of equations (2.1.8) and (2.1.9) then yields the following linearising function:

$$\boldsymbol{\Psi}^T\mathbf{I} = \frac{c_3}{c_4}\|\Psi\| + \frac{1}{2c_4T_\Psi}\left(\|\Psi\|_d - \|\Psi\|\right), \tag{2.1.10}$$

2b4) The master control law

The linearising functions (2.1.6) and (2.1.10) are now solved as two simultaneous equations in the two components of **I**, yielding the required control law. Thus:

$$\mathbf{I_d} = \frac{1}{\|\Psi^*\|}\begin{bmatrix} -\Psi_\beta^* & \Psi_\alpha^* \\ \Psi_\alpha^* & \Psi_\beta^* \end{bmatrix}\begin{bmatrix} \dfrac{1}{\tilde{c}_5}\left(\dfrac{\tilde{J}}{T_\omega}(\omega_d - \hat{\omega}_r) + \hat{\Gamma}_L\right) \\ \dfrac{\tilde{c}_3}{\tilde{c}_4}\|\Psi^*\| + \dfrac{1}{2\tilde{c}_4T_\Psi}\left(\|\Psi^*\|_d - \|\Psi^*\|\right) \end{bmatrix}, \tag{2.1.11}$$

where the ^ denotes estimated state variables and the ~ denotes assumed constant parameters. Also, the fictitious control vector, **I**, is replaced by the demanded current vector, $\mathbf{I}_d$, on the basis that the slave control law ensures $\mathbf{I} \cong \mathbf{I}_d$.

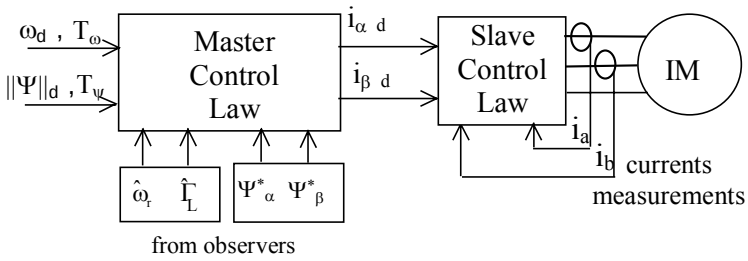

Fig. 2.1.1 Hierarchical structure of the control system

It should be noted that the constant external disturbance torque, $\hat{\Gamma}_L$, is treated as a state variable and estimated in the observer together with the other state variables.

2c) The slave control law

The sub-plant to be controlled here is defined by equation (2.1.3). Two options can be considered.

First for *simulation investigation only* a high gain proportional control law with saturation limits equal to the power supply voltages, $\pm U_s$, is formed. Thus:

$$\mathbf{U} = \text{sat}\left[G_I\left(\mathbf{I}_d - \mathbf{I}\right), \mathbf{U_s}\right] \tag{2.1.12}$$

where $\text{sat}\left(x, x_{sat}\right) \overset{\Delta}{=} \begin{cases} x, & |x| \le x_{sat} \\ x_{sat}\ \text{sgn}(x), & |x| > x_{sat} \end{cases}$, $\text{sgn}(x) \overset{\Delta}{=} \begin{cases} +1, & x \ge 0 \\ -1, & x < 0 \end{cases}$ and $\mathbf{U}_s = \left[u_{s\alpha}\ u_{s\beta}\right]^T$

where $U_{s\alpha} = U_{s\beta} = U_s$. The constant gain, G_I, is as high as possible but limited to $G_I < \left(2 - \tilde{c}_1 \tilde{a}_1 h\right)/\left(\tilde{c}_1 h\right)$ by the iteration period, h, of the digital processor.

The second option, which is for practical implementation, is the bang-bang control law:

$$\mathbf{U} = U_{max}\,\mathbf{sgn}\left[\mathbf{I}_d - \mathbf{I}\right] \tag{2.1.13a}$$

$$\begin{aligned} U_\alpha &= U_{max}\,\mathbf{sgn}\left[I_{\alpha d} - I_\alpha\right] \\ U_\beta &= U_{max}\,\mathbf{sgn}\left[I_{\beta d} - I_\beta\right] \end{aligned}, \tag{2.1.13b}$$

operating in the sliding mode, ideally maintaining $\mathbf{I}=\mathbf{I_d}$ with a finite but high switching frequency, limited by h, maintaining $\mathbf{I} \cong \mathbf{I}_d$. Since the controlled dynamics of equation (2.1.3) is only of first order, the *closed-loop* system has *zero order dynamics* between $\mathbf{I}_d$ and $\mathbf{I}$ meaning that in theory, as $h \rightarrow 0$, $\mathbf{I}$ follows $\mathbf{I}_d$ precisely with zero dynamic lag.

2d) Automatic Start Algorithm

The primary control law cannot initiate the rotor flux build-up unaided with zero initial state variables. This is evident in equation (2.1.11), which has a singularity at $\left\|\hat{\Psi}\right\| = \mathbf{0}$. This problem is overcome here by overriding the master control law with a simple algorithm (a slightly modified version of that previously published), which applies the maximum voltage under prescribed demanded values of currents until the estimated rotor magnetic flux norm has exceeded a designated minimum value, as follows:

$$\text{If } \left\|\hat{\Psi}\right\| < \|\Psi\|_{min} \text{ then } I_{d\_a} = I_{max} \text{ and } I_{d\_b} = I_{d\_c} = \frac{-I_{max}}{2} . \qquad (2.1.14)$$

2.1.3 State Estimation and Filtering

The rotor magnetic flux, rotor speed and load torque which are the inputs for the master control algorithm are produced by the following set of three observers. The first is the rotor magnetic flux estimator. The second is a stator current vector *pseudo sliding-mode* observer formulated for generation of an unfiltered estimate of the rotor speed. The third observer provides filtered rotor speed and load torque estimates, a direct measurement of load torque being assumed to be unavailable.

3a) The Rotor Magnetic Flux Estimator

For induction motors a means of estimating the rotor magnetic flux components may be devised by eliminating the, rotor speed, ω_r, between equations (2.1.2) and (2.1.3), yielding equation (2.1.15a):

$$\frac{d}{dt}\begin{bmatrix}\psi_\alpha\\ \psi_\beta\end{bmatrix}=\left(c_4-\frac{a_1}{c_2}\right)\begin{bmatrix}I_\alpha\\ I_\beta\end{bmatrix}+\left(\frac{1}{c_2}\right)\begin{bmatrix}U_\alpha\\ U_\beta\end{bmatrix}-\left(\frac{1}{c_1c_2}\right)\frac{d}{dt}\begin{bmatrix}I_\alpha\\ I_\beta\end{bmatrix}, \qquad (2.1.15a)$$

from which

$$\begin{bmatrix}\psi^*_\alpha\\ \psi^*_\beta\end{bmatrix}=\int\left[\left(\tilde{c}_4-\frac{\tilde{a}_1}{\tilde{c}_2}\right)\begin{bmatrix}I_\alpha\\ I_\beta\end{bmatrix}+\left(\frac{1}{\ddot{c}_2}\right)\begin{bmatrix}U_\alpha\\ U_\beta\end{bmatrix}\right]dt-\left(\frac{1}{\tilde{c}_1\tilde{c}_2}\right)\begin{bmatrix}I_\alpha\\ I_\beta\end{bmatrix}. \qquad (2.1.15b)$$

With zero initial conditions, all the quantities on the right hand side of equation (2.1.15b) are known, but the pure integration would be subject to drift in practice. This problem is overcome here by noting that $\int_0^\infty \boldsymbol{\Psi}(t)dt=\mathbf{0}$. Accordingly, if $\|\Psi\|$ exceeds $(1+\lambda)\|\Psi\|_d$ where $0<\lambda<1$, the drift is prevented by replacing the integral of equation (16) by a first order filter with a time constant, T_q such that $T_q >> 1/\omega_{r\,min}$, where $\omega_{r\,min}$ is the lowest angular velocity envisaged for the particular application. This is realised by numerical integration of the following differential equation, replacing the true constant parameters by their estimates:

$$\dot{\mathbf{Q}}+\frac{1}{2T_q}\left(1+\mathrm{sgn}\left(\|\hat{\Psi}\|-(1+\lambda)\|\Psi\|_d\right)\right)\mathbf{Q}=\left(\tilde{c}_4-\frac{\tilde{a}_1}{\tilde{c}_2}\right)\mathbf{I}+\left(\frac{1}{\tilde{c}_2}\right)\mathbf{U}. \qquad (2.1.16)$$

Equation (2.1.17), completes the algorithm as follows:

$$\hat{\boldsymbol{\Psi}}=\mathbf{Q}-\left(\frac{1}{\tilde{c}_1\tilde{c}_2}\right)\mathbf{I}. \qquad (2.1.17)$$

3b) The Pseudo Sliding Mode Observer and Angular Velocity Extractor

A stator current *pseudo-sliding-mode* observer is formulated for generation of an unfiltered estimate, $\tilde{c}_1\tilde{c}_2\mathbf{P}(\hat{\omega}_r)\hat{\boldsymbol{\Psi}}$, of the term, $c_1c_2\mathbf{P}(\omega_r)\boldsymbol{\Psi}$, of equation (2.1.3), using the *equivalent control method* [3]. The observer is therefore formed as a stator current real time model but *purposely omitting terms containing* ω_r.

Thus:

$$\dot{\mathbf{I}}^* = \tilde{c}_1\left[-\tilde{a}_1\mathbf{I}^* + \mathbf{U}\right] - \mathbf{v} \tag{2.1.18a}$$

$$\begin{aligned} I_\alpha^* &= \tilde{c}_1\left[-\tilde{a}_1 I_\alpha^* + U_\alpha\right] - v_\alpha \\ I_\beta^* &= \tilde{c}_1\left[-\tilde{a}_1 I_\beta^* + U_\beta\right] - v_\beta \end{aligned} \tag{2.1.18b}$$

$$\mathbf{v} = -\mathbf{v}_{max}\,\mathrm{sgn}\left[\mathbf{I}^* - \mathbf{I}\right] \tag{2.1.19a}$$

$$\begin{bmatrix} v_{eq\,\alpha} \\ v_{eq\,\beta} \end{bmatrix} = -v_{max} \cdot \mathrm{sgn}\begin{bmatrix} i_\alpha - i_\alpha^* \\ i_\beta - i_\beta^* \end{bmatrix}, \tag{2.1.19b}$$

where $\mathbf{v}^T = [v_\alpha \;\; v_\beta]$ are the model corrections, i_α^* and i_β^*, are estimates of i_α and i_β, as in conventional observers. The useful observer outputs here, however, are the continuous *equivalent values* $\mathbf{v}_{eq}$, (*i.e., the short term mean values*) [3], of the rapidly switching **v**. But equation (2.1.19) cannot directly generate the equivalent values. Instead, a *pseudo-sliding-mode* observer may be formed by replacing the signum functions by high gains (2.1.20):

$$\mathbf{v}_{eq} = \mathbf{K}_{SM}\left[\mathbf{I}^* - \mathbf{I}\right] \tag{2.1.20a}$$

$$\begin{bmatrix} v_{eq\,\alpha} \\ v_{eq\,\beta} \end{bmatrix} = K_{sm} \cdot \begin{bmatrix} i_\alpha - i_\alpha^* \\ i_\beta - i_\beta^* \end{bmatrix}, \tag{2.1.20b}$$

where $\mathbf{K}_{SM} = \begin{bmatrix} k_{SM1} & 0 \\ 0 & k_{SM2} \end{bmatrix}$ so that **v** is continuous and closely approaches $\mathbf{v}_{eq}$ for sufficiently high gains, limited only by the non-zero iteration interval, h, of the digital implementation ($k_{SMq} < \left(2 - \tilde{c}_1\tilde{a}_1 h\right)/h$, $q = 1, 2$ with Euler explicit numerical integration). The resulting approximation to $\mathbf{v}_{eq}$ is denoted $\mathbf{v}_{eq}^*$. Assuming that observer (2.1.19) operates in the ideal sliding mode, $\mathbf{v} = \mathbf{v}_{eq}$ if $\mathbf{I}^* = \mathbf{I}$ and $\dot{\mathbf{I}}^* = \dot{\mathbf{I}}$. Then the right hand sides of equations (2.1.3) and (2.1.18) may be equated, yielding (with $\mathbf{v}_{eq}$ replaced by $\mathbf{v}_{eq}^*$):

$$\tilde{c}_1\left[-\tilde{a}_1\mathbf{I}^* + \mathbf{U}\right] - \mathbf{v}_{eq}^* = c_1\left[c_2\mathbf{P}(\omega_r)\boldsymbol{\Psi} - a_1\mathbf{I} + \mathbf{U}\right]. \tag{2.1.21}$$

A formula for $\mathbf{v}_{eq}^*$ is then formed by assuming $\tilde{c}_1 = c_1$, $\tilde{c}_2 = c2$, $\tilde{a}_1 = a_1$ and $\mathbf{I}^* = \mathbf{I}$.

Replacing $\boldsymbol{\Psi}$ and ω_r in equation (2.1.21), by their estimates $\boldsymbol{\Psi}^*$ and $\hat{\omega}_r$ yields:

$$\mathbf{v}_{eq}^* = -\tilde{c}_1\tilde{c}_2\mathbf{P}(\hat{\omega}_r)\boldsymbol{\Psi}^* \tag{2.1.22a}$$

$$\begin{bmatrix} v_{eq\,\alpha}^* \\ v_{eq\,\beta}^* \end{bmatrix} = \tilde{c}_1 \quad \tilde{c}_2 \begin{bmatrix} \tilde{c}_3 & p\hat{\omega}_r \\ -p\hat{\omega}_r & \tilde{c}_3 \end{bmatrix} \cdot \begin{bmatrix} \psi_\alpha^* \\ \psi_\beta^* \end{bmatrix} \tag{2.1.22b}$$

The following formula for the desired angular velocity estimate, ω_r^*, is then derived from the components, $\mathbf{v}^*_{eq}$ of equation (2.1.22b):

$$\omega_r^* = \frac{-v_{eq\,\alpha}^*\,\psi_\beta^* + v_{eq\,\beta}^*\psi_\alpha^*}{c_1c_2p\cdot\left\|\Psi^*\right\|}\cdot \tag{2.1.23}$$

A block diagram of the pseudo-sliding mode observer is shown in Fig. 2.1.2a.

3c) Observer for Load Torque Estimation and Rotor Speed Estimate Filtering

The load torque estimate required by the master control law is provided here by a standard observer having a similar structure to a Kalman filter, a direct measurement of this being assumed to be unavailable. The real time model of this observer is based on motor torque equation (2.1.1). The load torque is treated as a state variable whose differential equation augments the real time model [3]. In this case, the load torque is assumed constant in the formulation of the real time model and so its state differential equation is simply $\dot{\Gamma}_L = 0$. The observer correction loop is actuated by the error between the rotor speed estimate, ω^*_r, from the angular velocity extractor and the estimate, $\hat{\omega}_r$, from the real time model. Since $\hat{\omega}_r$ is a filtered version of ω^*_r it is used directly in the master control law instead of ω^*_r. The continuous time version of this observer is therefore:

$$\begin{aligned} e_\omega &= \omega_r^* - \hat{\omega}_r \\ \dot{\hat{\omega}}_r &= \frac{1}{J}\left\{ \frac{3L_m}{2L_r}p\left[\psi_\alpha i_\beta - \psi_\beta i_\alpha\right] - \Gamma_L \right\} + k_\omega e_\omega \\ \dot{\hat{\Gamma}}_L &= k_\Gamma e_\omega \end{aligned} \tag{2.1.24}$$

Block diagram of filtering observer is shown in Fig. 2.1.2b.

The observer poles are both placed at $s = -1/T_f$ so that the filtering time constant, T_f, is a single design parameter for the gains, k_ω and k_Γ as it is shown in (2.1.25a), where the right hand side of equation is the characteristic equation of the filtering observer characteristic polynomial:

$$s^2 + \frac{2}{T_f}s + \frac{1}{T_f^2} = s^2 + k_\omega s + \frac{k_\Gamma}{J} \qquad (2.1.25a)$$

$$k_\omega = \frac{2}{T_f} \qquad k_\Gamma = \frac{J}{T_f^2}. \qquad (2.1.25b)$$

Although the load torque is assumed constant in the formulation of the real time model of the observer, the estimate, $\hat{\Gamma}_L$, will follow a time varying load torque and will do so more faithfully as T_f is reduced, but at the expense of sensitivity to any noise contaminating the rotor speed estimate, ω_r^*. It may be shown that any driven mechanical load can be represented by a time varying load torque component. It follows that since the control system is designed to be insensitive to a time varying load torque, it will also be insensitive to the dynamics of the driven mechanical load. The control system therefore offers robustness.

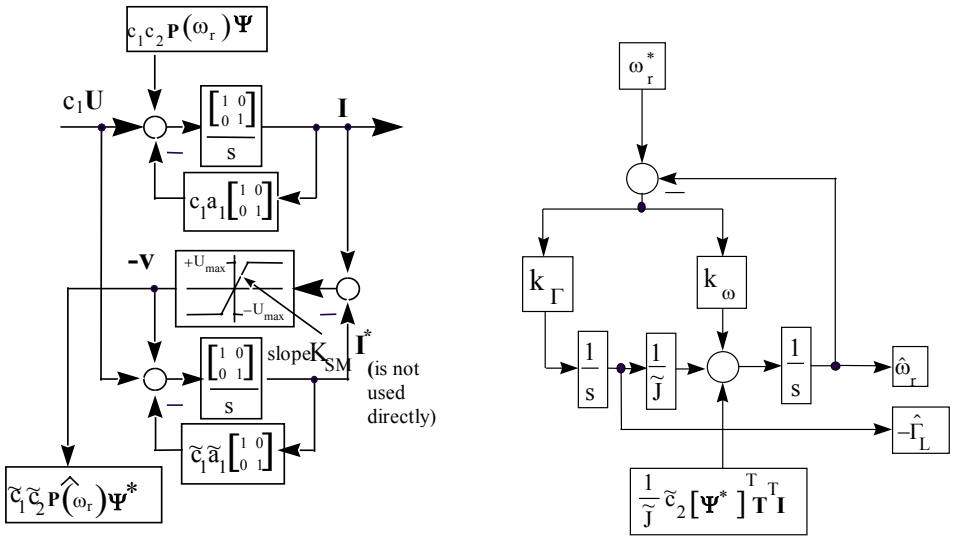

a) Pseudo-sliding mode observer *b) Filtering observer*

Fig. 2.1.2 Block diagrams of pseudo-sliding mode observer and filtering observer

The system can be completed with the rotor magnetic flux filtering observer which is based on equation (2.1.2), the inputs being the filtered angular velocity estimate, $\hat{\omega}_r$, together with $\mathbf{I}$ and $\boldsymbol{\Psi}^*$:

$$\dot{\hat{\boldsymbol{\Psi}}} = -\mathbf{P}(\hat{\omega}_r)\hat{\boldsymbol{\Psi}} + \tilde{c}_4\mathbf{I} + \mathbf{K}_\psi\left(\boldsymbol{\Psi}^* - \hat{\boldsymbol{\Psi}}\right) \tag{2.1.26}$$

The observer may be made time invariant with a filtering time constant of T_{mg} by the following gains:

$$\mathbf{K}_\Psi = \begin{bmatrix} 1/T_{mg} & 0 \\ 0 & 1/T_{mg} \end{bmatrix} - \mathbf{P}(\hat{\omega}_r). \tag{2.1.27}$$

This yields the following dynamics equation for the estimation error, :

. (2.1.28)

The above observers must be converted to the discrete time form for digital implementation [4].

Finally, Fig. 2.1.3 shows the complete control system.

Fig. 2.1.3 Overall control system block diagram

2.1.4 Alternative Load Torque Compensating Schemes

Results with the filtering observer (2.1.24), Fig. 2.1.2b were only available as simulations during the initial experimental period. The first experimental results were produced with the aid of a PID controller in which the integrator output effectively performed the combined function of load torque estimation and correction, as shown in Fig. 2.1.4. Without the filtering observer then, ω^*_r was fed to control law (2.1.11) instead of the filtered version, $\hat{\omega}_r$.

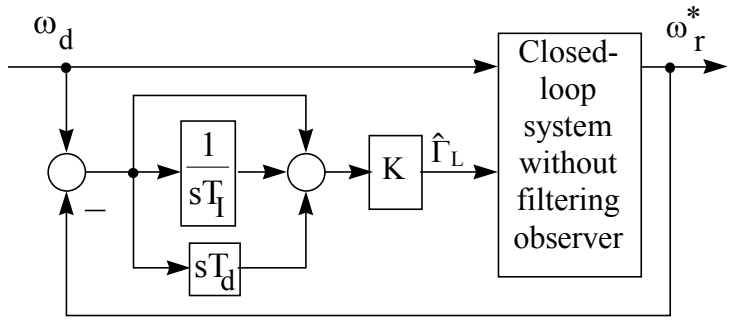

Fig. 2.1.4 Load torque compensation by outer PID control loop

This was successful. A more elegant solution than the somewhat heuristic PID control loop, however, was pursued later, as follows. It was observed that with $\hat{\Gamma}_L = 0$ in control law (2.1.11), the correct exponential form of speed step response was obtained but with a steady state error. Under these circumstances, the response to a step speed reference input appeared to correspond to a system with transfer function:

$$\frac{\omega_r(s)}{\omega_d(s)} = \frac{k}{1+sT_\omega}, \tag{2.1.29}$$

where $0 < k < 1$. This observation lead to a system based on a special form of sliding mode control embodying a *control smoothing integrator* [8]. Conventional sliding mode control employs bang-bang control action with output derivative feedback to achieve a closed-loop dynamic performance virtually independent of the plant parameters, the number of output derivatives being equal to the 'r-1', where r is the plant rank. The control chatter is eliminated by inserting an integrator between the bang-bang control element and the control input and treating the input to the integrator as a new control variable, one more derivative being added to the

output feedback. In this case, the closed-loop system (2.1.29) is treated as a new plant to be controlled. This, together with the additional integrator is of rank 2 and so derivative $\dot{\omega}^*_r$ is required (generated by software differentiation) as well as ω^*_r in the output feedback. Since, in this case, there is no need for the bang-bang control action, it is replaced by a high gain, K, and this is well known to produce a similar dynamic performance. The result is an outer loop closed around the existing system, as shown in Fig. 2.1.5.

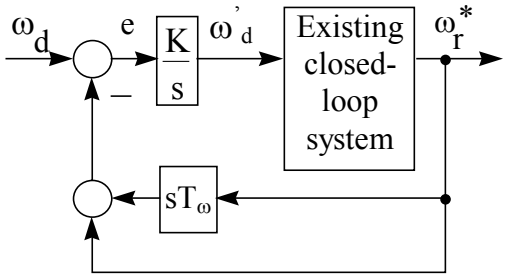

Fig. 2.1.5 Load torque compensation by high gain outer control loop

The speed demand, ω_d, is then applied to the high gain outer loop controller and the output of this is the speed demand, ω'_d , of the existing closed loop system, as shown. In theory, the system of Fig. 2.1.5 is stable for any gain, K. Hence, if the gain, K, is increased sufficiently, then the error, e, is driven to zero. In this case, it may easily be shown that the closed-loop system obeys transfer function (2.1.29) with k=1, as desired.

2.1.5 Experimental Results

The experimental equipment for evaluation of the new control strategy for electric drives with induction motors includes an induction motor with nominal power, P_n= 120 W, equipped with an eddy-current brake for applying an external load torque. A complete set of the motor parameters may be found in the Appendix. An inverter bridge with IGBT transistors (*parameters in appendix*) and an IR 2130 driver was employed. A Pentium P130 computer carried the control algorithms under evaluation. This was equipped with a PCL812/PG PC-lab card for sensing the currents of two-phases via LEM current sensors, the third phase current being computed.

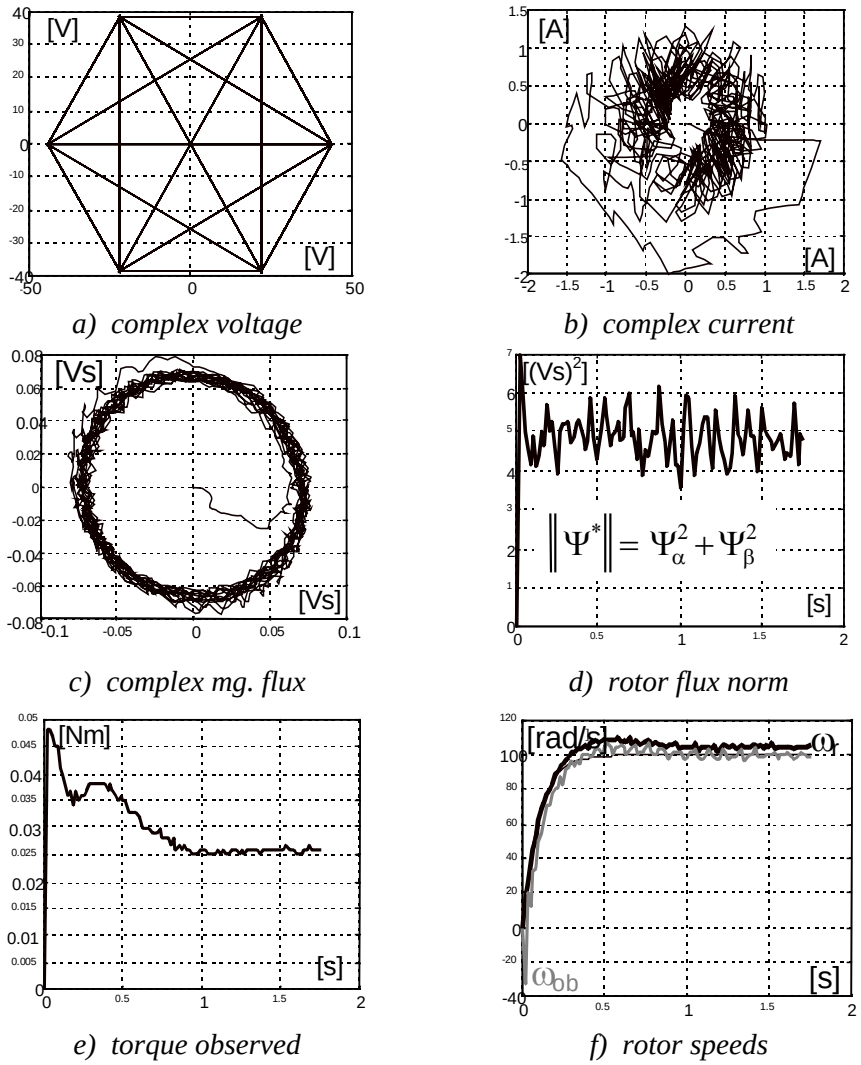

a) complex voltage *b) complex current*

c) complex mg. flux *d) rotor flux norm*

e) torque observed *f) rotor speeds*

Fig. 2.1.6 Experimental results for idle running induction motor

The sampling frequency was limited to 7 kHz, mainly due to the relatively slow A/D converters of the PC-lab card. In fact, the conversion of the current measurements into digital form occupied 80% of the computational cycle. For further experiments, the faster PCL818 PC-Lab card is recommended together with a dedicated DSP or microprocessor.

Experimental results for the idle running motor with the PID load torque estimator/corrector of Fig. 2.1.4 are shown in Fig. 2.1.6. The speed and flux magnitude reference inputs, are, respectively, $\omega_d = 100$ rad/s, and $||\Psi||_d = 5\text{e-}3\ (\text{Vs})^2$ with prescribed time constants of $T_\omega = 0{,}1$ s, for rotor speed and $T_\Psi = 5\text{e-}3$ s for the rotor magnetic flux norm, to ensure fast excitation of the motor.

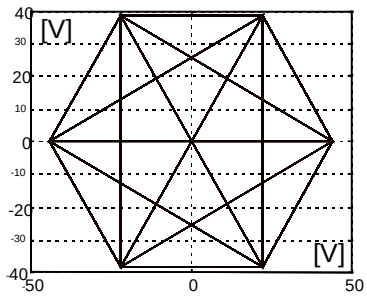

a) complex voltage

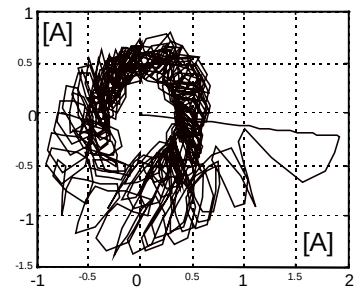

b) complex current

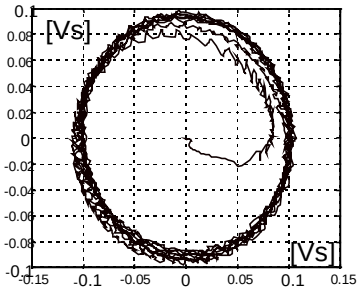

c) complex mg. flux

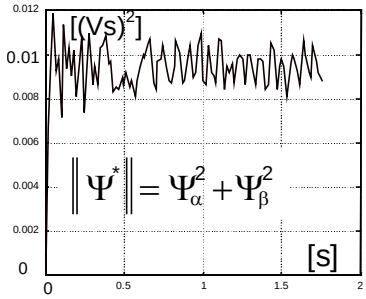

d) rotor flux norm

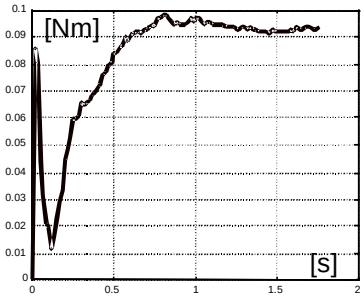

e) torque observed

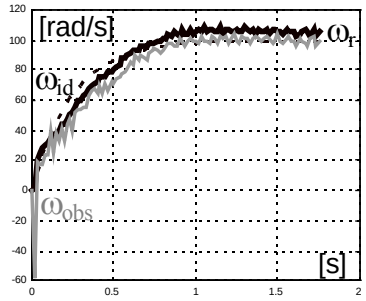

f) rotor speeds

Fig. 2.1.7 Experimental results for loaded induction motor

All the experiments were carried out with a dc supply of U_{dc}=60 V, corresponding to 40 V magnitude of phase voltage. This was the main reason for reducing the maximum torque well below the specified nominal torque. The rotor speed was monitored by means of a tacho-dynamo for comparison with the ideal response yielded by equation (2.1.5), which was computed in real time during the experiments. These variables are plotted on the speed response graph together with the speed estimate from the filtering observer.

Experimental results for the loaded induction motor are shown in Fig. 2.1.7, again with the PID load torque estimator/corrector of Fig. 2.1.4. The rotor magnetic flux reference input in this case was increased to $||\Psi||_d$ = 1e-2 $(Vs)^2$ and the corresponding time constant was T_Ψ = 5e-3 s. The rotor speed parameters were ω_d = 100 rad/s and the time constant was increased to T_ω = 0,3 s. It was found necessary to make small adjustments to the parameters of the PID load torque estimator/corrector to obtain good results.

The real rotor speed response does not show a significant deviation from the ideal speed response as evident in Fig. 2.1.7 (f). This indicates that the PID load torque estimator is a strong candidate for later consideration and the experimental drive performance should be carefully examined against that which will be obtained with the originally intended filtering observer in the future.

Step changes in speed demand, *including changes of direction,* also with the PID load torque estimator, are shown in Fig. 2.1.8. Despite some problems with load torque computation when the angular speed approached zero value, there is not a remarkable difference between ideal angular speed response and the real rotor speed response.

a) speed changes *b) speed reverse*

Fig. 2.1.8 Responses to step changes in rotor speed reference inputs

Experimental results with the high gain outer control loop of Fig. 2.1.5 are presented in Fig. 2.1.9. It should be noted that similar results to those of Fig. 2.1.6 and Fig. 2.1.7 were obtained under the same test conditions. It was then decided to test the system robustness by applying a step change of load torque at about 0,5 s.

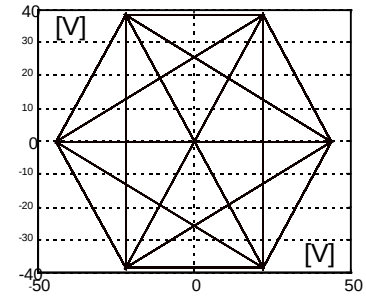

a) complex voltage

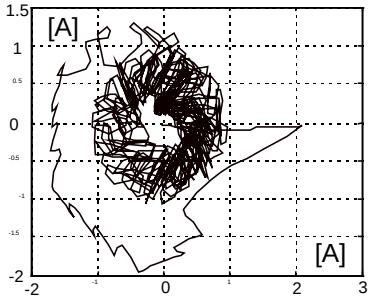

b) complex current

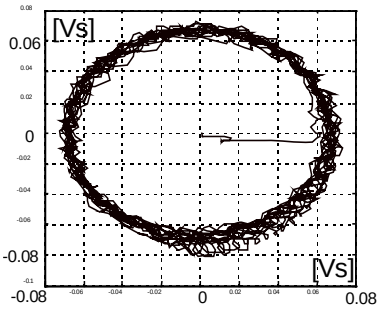

c) complex mg. flux

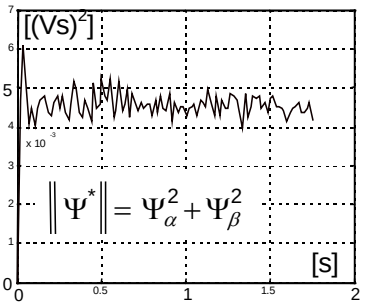

d) rotor flux norm

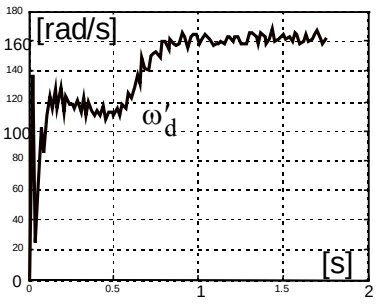

e) speed demand

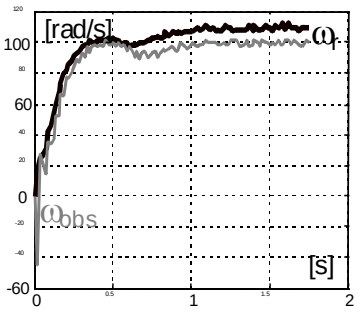

f) rotor speeds

Fig. 2.1.9 Experimental results for step change of load of induction machine

As seen in Fig. 2.1.9 (e), the transient load torque is compensated by a higher value of the demanded speed, ω_d, and the real speed response keeps fairly close to the ideal speed response, as shown in Fig. 2.1.9 (f).

These experimental results show that moderate speed control accuracy may be achieved with the scheme of Fig. 2.1.4 as well as that of Fig. 2.1.5. It is important to emphasise that the PID solution required considerable tuning time, in contrast to the high gain solution, which entailed only increasing K within practical limits.

2.1.6 Conclusions and Recommendations for Further Work

The experimental results show good agreement with the theoretical ones previously described in [5] and [6].

The implementation of the system with the original filtering observer for speed and load torque estimation should be carried out and the results carefully compared with those obtained with the alternative schemes.

Further improvement of the induction motor control could be investigated with a modified algorithm for control of the rotor speed and direct control of the angle between the rotor magnetic flux and stator current vectors, as it was suggested for the synchronous motor in [7].

The general approach presented here should be pursued experimentally for synchronous motor drives. In fact, preliminary experimental results have already been obtained and these are encouraging.

Implementation of more sophisticated inverter modulation techniques, such as space vector control, should also be carried out, since this can bring about significant improvements of harmonic content of the inverter output currents, which will improve the performance of the observers responsible for producing the flux and speed estimates on which the control law depends.

2.1.7 References

[1] DODDS, S. J., VITTEK, J.: '*Centring Control System for the Reaction Sphere utilising Electromagnetic Induction Actuators*'. Proceedings of *ELECTRO'95 International Conference of Faculty of Electrical Engineering*, Sept. 1995, Zilina, Slovakia, pp. 144 - 150.

[2] DRAKUNOV, S. V., IZOSIMOV, D. B., LUK'YANOV, A. G., UTKIN, V. A., UTKIN, V. I.: '*The block control principle, I, II*'. *Automation and Remote Control,* Vol. 45, No. 5, Part 1, 1990, pp. 601 - 609.

[3] UTKIN, V. A.: '*Method of separation of motions in observation problems*'. *Automation and Remote Control,* Vol. 44, No. 12, Part 1, 1990, pp. 300 - 308.

[4] KWAKERNAA,K. H., SIVAN, R.: '*Linear Optimal Control Systems*'. Wiley-Interscience, New York-London-Sydney-Toronto, 1972.

[5] DODDS, S. J., UTKIN, V. A., VITTEK, J.: '*A Motion Separation Method for the Control of Induction Motors with Prescribed Closed-Loop Dynamics*'. *NOLCOS '95*, *IFAC Conference on Non-Linear Control Systems*, Tahoe City, CA, USA, Vol. 2, 1995, pp. 816 - 821.

[6] DODDS, S. J., UTKIN, V. I., VITTEK, J., MIENKINA, M.: '*Simulation of a new sensorless induction motor drive with prescribed closed loop dynamics*'. Proceedings of *An International Scientific Conferece on Computer Science*, University of Ostrava, Czech Republic, 1995, pp. 187 - 195.

[7] DODDS, S. J, UTKIN, V. A., VITTEK, J.*: 'Self Oscillating, Synchronous Motor Drive Control System with Prescribed Closed-Loop Speed Dynamics*'. Proceeedings of ***2nd*** *EPE Chapter Symposium on Electric Drive Design and Applications*, Nancy, France, 4-6 June, 1996, pp. 23 - 28.

[8] DODDS, S. J. and WALKER, A. B.: '*Three axis Sliding Mode Attitude Control of Rigid-body Spacecraft with Unknown Dynamic Parameters*'. *International Journal of Control,* Vol. 54. No. 4, pp. 41 - 54.

Appendix

The three-phase induction motor PARVALUX parameters are as follows:

Induction motor parameters		**Equivalent circuit parameters**	
Rated power	P_n=120 W	Mutual inductance	L_m=21 mH
Rated speed	n_n=1410 rpm	Stator inductance	L_s=24,6 mH
Rated current	Y/Δ I_n=1,2/1,9 A	Rotor inductance	L_r=24,6 mH
Terminal voltage	Y/Δ U_n=87/50 V	Stator resistance	R_s=11,16 Ω
Moment of inertia	J=1,7e-4 kgm^2	Rotor resistance	R_r=12,53 Ω
Parameters of IGBT FUJI 6MBI-060		**Current sensors LEM**	
Rated voltage	600 V	LTA 50P/SPI	
Rated current	6x10 A		

Acknowledgement

The authors wish to thank the INTAS Association, Brussels, for their support of this research, which was carried out within the INTAS93-317 project.